


# Optics Letters

## Calculation model of dense spot pattern multi-pass cells based on a spherical mirror aberration

RUYUE CUI,<sup>1,2</sup> LEI DONG,<sup>1,2,\*</sup> HONGPENG WU,<sup>1,2</sup> SHANGZHI LI,<sup>1,2</sup> XUKUN YIN,<sup>1,2</sup> LEI ZHANG,<sup>1,2</sup> WEIGUANG MA,<sup>1,2</sup>  WANGBAO YIN,<sup>1,2</sup> AND FRANK K. TITTEL<sup>3</sup>

<sup>1</sup>State Key Laboratory of Quantum Optics and Quantum Optics Devices, Institute of Laser Spectroscopy, Shanxi University, Taiyuan 030006, China

<sup>2</sup>Collaborative Innovation Center of Extreme Optics, Shanxi University, Taiyuan 030006, China

<sup>3</sup>Department of Electrical and Computer Engineering, Rice University, 6100 Main Street, Houston, Texas 77005, USA

\*Corresponding author: donglei@sxu.edu.cn

Received 20 December 2018; accepted 23 January 2019; posted 25 January 2019 (Doc. ID 355905); published 19 February 2019

We report a novel calculation model for dense spot pattern multi-pass cells consisting of two common identical spherical mirrors. A modified ABCD matrix without the paraxial approximation was developed to describe the ray propagation between two spherical mirrors and the reflection on the mirror surfaces. The intrinsic aberration from the spherical curvature creates a set of intricate variants with respect to a standard Herriot circle spot pattern. A series of detailed numerical simulations are implemented to verify that the input and output beams remain the same and, hence, retrace the same ray pattern. The set of exotic spot patterns obtained with a high fill factor improves the utilization efficiency of the mirror surfaces and produces a longer total optical path length with a low mirror cost. © 2019 Optical Society of America

<https://doi.org/10.1364/OL.44.001108>

Multi-pass cells (MPCs) with a long effective optical path length constructed with highly reflective mirrors are widely used in optical absorption spectroscopy and gas-phase optical delay lines for the detection of trace amounts of gas molecules [1–7]. Early spherical MPCs developed by White [8] and Herriot [9] are still in use in a laser-based spectroscopic trace gas sensor due to their simplicity, reliability robustness, and operability [10,11]. In order to improve the utilization efficiency of mirror surfaces and, hence, obtain a longer optical path length, Herriot described astigmatic MPCs in which the  $x$ - $z$  and  $y$ - $z$  planes of spherical mirror have different focal lengths, thus creating Lissajous spot patterns. As a result, this increases the number of the ray reflection in a MPC, while minimizing the spot overlap [12]. Recently, many variants based on the astigmatic MPCs were reported with a similar high fill factor pattern, in which at least one spherical mirror was replaced with a cylindrical mirror [13,14]. In 2017, Ozharar *et al.* [15] designed an aspherical mirror whose focal length varies inversely as the ray height from the optical axis. With an appropriate incident angle and position of a ray, a rich set of dense patterns was achieved.

However, so far, MPCs with the most dense patterns are based on aspherical mirrors. In practice, mirrors with high surface accuracy are manufactured by grinding and polishing techniques that naturally produce spherical surfaces. The manufacture of aspheric surfaces is more complex, and it is difficult to produce a mirror of sufficient surface accuracy to follow the designed pattern. Therefore, spherical mirrors are required in these MPCs due to the simplicity, more easily controlled surface quality, and more importantly lower cost.

As shown in Fig. 1, the incident ray transmits between two mirrors (M1 and M2) and then reflects on the M2 surface to complete a pass count in the simple structure of a two-spherical-mirror MPC. With conventional calculations of ray tracing analysis, the paraxial theory was used with two assumptions: (1) the optical path lengths of any rays between two mirrors,  $d_n$ , are constant,  $D$ , where  $n$  is the pass count; and (2) all the rays make small angles to the optic axial of the system, so that three important angle approximations are valid, i.e.,  $\sin \theta \approx \theta$ ,  $\tan \theta \approx \theta$ , and  $\cos \theta \approx 1$ . However, with more highly curved surfaces, particularly marginal rays, and more pass counts, the paraxial theory generates increasingly large deviations from the actual performance due to spherical aberrations. For example,

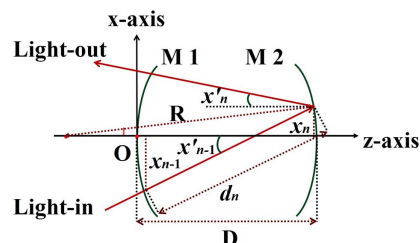


**Fig. 1.** Transmission of rays between two identical spherical mirrors, M1 and M2, and the reflection on the M2 surface, in the  $x$ - $z$  plane of a Cartesian coordinate system.  $R$ , radius of the curvature of the spherical mirrors;  $D$ , mirror spacing;  $O$ , origin of coordinates;  $d_n$ , optical path length for the  $n$ th transmission between M1 and M2;  $(x_{n-1}, x'_{n-1})$ , spot location on M1 and initial ray inclination angle;  $(x_n, x'_n)$ , spot location on M2 and the ray inclination angle after  $n$ th transmitting between M1 and M2 and reflected by M2.

at an angle of  $10^\circ$ , the paraxial approximation of  $\sin \theta \approx \theta$  has an error of 0.5%, where these errors are not accounted for in the standard ABCD matrix. With an increasing pass count, these errors will be accumulated and amplified, and distort the real pattern. The presence of paraxial approximation and a lack of equation-based designs that match the actual ray trajectories in MPC limit the ability to develop other spot patterns that may provide other viable MPC arrangements. In particular, the lack of consideration of spherical aberration effects, which are not easily simulated in conventional matrix-based approaches, is a major limitation of these design endeavors.

In this Letter, we report a novel dense pattern MPC design using two common identical spherical mirrors. An accurate ABCD matrix without the paraxial approximation was developed to describe the propagation of both the paraxial and marginal rays between the two spherical mirrors and the reflection of these rays on a mirror surface. A rich set of spot patterns on the mirrors can be created by numerical simulations due to the presence of the spherical aberrations. These novel spot distributions from a simpler mirror surface curvature and with a lower cost have the similar patterns as those obtained by Ozharar *et al.* [15], who used an aspherical mirror designed with varying focal lengths.

The reported MPC was assumed to consist of two identical spherical mirrors. In the paraxial analysis of a two-spherical-mirror MPC, the ABCD matrix describing one pass count consists of a standard transmission matrix and a standard reflection matrix:

$$\begin{bmatrix} A & B \\ C & D \end{bmatrix} = \begin{bmatrix} 1 & 0 \\ -2/R & 1 \end{bmatrix} \cdot \begin{bmatrix} 1 & D \\ 0 & 1 \end{bmatrix}. \quad (1)$$

In order to remove the paraxial approximation, we define two operators  $S$  and  $L$ , which are  $S\varphi = \sin \varphi$  and  $L\varphi = -2 \arcsin(\varphi/R)$ , respectively, where  $\varphi$  is an arbitrary rational number. Therefore, the new ABCD matrix describing one pass count without the paraxial approximation can be expressed as

$$\begin{bmatrix} A & B \\ C & D \end{bmatrix} = \begin{bmatrix} 1 & 0 \\ L & 1 \end{bmatrix} \cdot \begin{bmatrix} 1 & d_n S \\ 0 & 1 \end{bmatrix}. \quad (2)$$

An iterative scheme is used to calculate the ray parameters for each pass count due to the fact that the modified ABCD matrix varies with each pass count. Using a Cartesian coordinate system, a ray before the transmission and reflection between the  $(n-1)$ th and the  $n$ th pass count is described by the coordinates  $(x_{n-1}, y_{n-1})$  of the point where it is located on the mirror surface of M1 or M2, and for which the ray has the inclination angles  $(x'_{n-1}, y'_{n-1})$ , as depicted in Fig. 1. The corresponding ray parameters after the  $n$ th pass count are calculated using the new ABCD matrix as follows:

$$\begin{aligned} x_n &= x_{n-1} + d_n \cdot \sin x'_{n-1}; & x'_n &= -2 \cdot \arcsin x_n/R + x'_{n-1}, \\ y_n &= y_{n-1} + d_n \cdot \sin y'_{n-1}; & y'_n &= -2 \cdot \arcsin y_n/R + y'_{n-1}. \end{aligned} \quad (3)$$

The above iterative equations can be carried out as long as  $d_n$  for each pass count is obtained.

If an incident ray enters the MPC from M1 with the initial location  $(x_0, y_0)$  on the M1 surface and inclination angles  $(x'_0, y'_0)$ , the location  $z_0$  on the M1 surface and the rest inclination angle  $z'_0$  can be calculated using the spherical equation for M1:

$$\begin{aligned} z_0 &= R - \sqrt{R^2 - x_0^2 - y_0^2}, \\ z'_0 &= \arcsin \sqrt{1 - (\sin x'_0)^2 - (\sin y'_0)^2}. \end{aligned} \quad (4)$$

Hence,  $z_n$  can be expressed by solving the line-sphere intersections:

$$z_n = (\sin z'_{n-1})^2 \cdot \left( -b_n/2 + (-1)^{n-1} \cdot \sqrt{(b_n/2)^2 - a_n \cdot c_n} \right), \quad (5)$$

where  $a_n$ ,  $b_n$ , and  $c_n$  are given by

$$\begin{aligned} a_n &= (\sin z'_{n-1})^{-2}, \\ b_n &= \left\{ \frac{x_{n-1} \cdot \sin x'_{n-1} + y_{n-1} \cdot \sin y'_{n-1}}{\sin z'_{n-1}} + \left( 1 - \frac{1}{(\sin z'_{n-1})^2} \right) \cdot z_{n-1} \right\} \cdot 2, \\ c_n &= \left\{ \left( x_{n-1} - \frac{\sin x'_{n-1}}{\sin z'_{n-1}} \cdot z_{n-1} \right)^2 + \left( y_{n-1} - \frac{\sin y'_{n-1}}{\sin z'_{n-1}} \cdot z_{n-1} \right)^2 \right\} \\ &\quad + \left( \frac{1+(-1)^{n-1}}{2} \cdot D + (-1)^n \cdot R \right)^2 - R^2 \end{aligned} \quad (6)$$

The optical path length for each pass count can be expressed as

$$d_n = (z_n - z_{n-1}) / \sin z'_{n-1}. \quad (7)$$

Thus,  $z'_n$  can be calculated using the results from Eq. (3):

$$z'_n = \frac{\arcsin \sqrt{1 - (\sin x'_n)^2 - (\sin y'_n)^2}}{(-1)^n}. \quad (8)$$

We first compared the calculated difference from the standard ABCD matrix Eq. (1) and the modified ABCD matrix without the paraxial approximation of Eq. (2). Two identical spherical mirrors with 25 mm focal length and 35.5 mm mirror spacing were employed. The initial location and inclination angles are  $(-8.5, 4.1 \text{ mm})$  and  $(16.1^\circ, 8.1^\circ)$ , respectively. The result from Eq. (1) shows a standard  $2 \times 2 \text{ cm}^2$  Herriot pattern as depicted in Fig. 2(a), while the result from Eq. (2) displays a spot pattern consisting of five arcs, as shown in Fig. 2(b). The spherical aberration makes the symmetrical Herriot distribution spots from a paraxial calculation yield five separated arcs. Therefore, when a marginal ray with a large inclination angle enters a MPC comprising two spherical mirrors, the aberration must be taken into account. The modified ABCD matrix can perform a calculation of ray tracing and describe the gradual evolution of the spot patterns on the mirror surface, which is a practical design tool. Subsequently the parameters of spherical mirrors were changed to 200 mm focal length and 266.3 mm mirror spacing. The small inclination angles  $(-3.4^\circ, 0^\circ)$  and initial location  $(8.1, -10.8 \text{ mm})$  were employed. The result from Eq. (2) in Fig. 2(d) is in excellent agreement with that from Eq. (1) in Fig. 2(c), which verifies that the modified ABCD matrix can return to the standard ABCD matrix with a small angle incident ray.

Numerical solutions were investigated for two-spherical-mirror MPCs with different entry beam parameters. An abundant set of exotic dense spot patterns generated by Eq. (3) is plotted in Fig. 3. In order to demonstrate that the two spherical mirrors have the powerful ability to create a set of intricate spot patterns that is the same as for aspherical mirrors, the four plots in Fig. 3 depicted similar spot patterns, as in Fig. 4 of Ref. [15], where an aspherical mirror was employed. All spots on the two

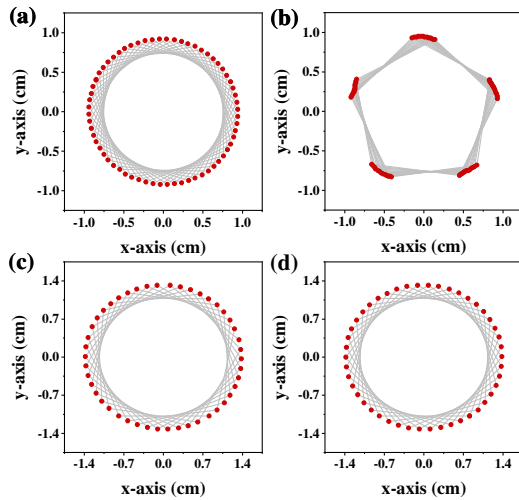


**Fig. 2.** Standard Herriot spot patterns produced by a conventional ABCD matrix with (a) large and (c) small angle incident rays. The corresponding spot patterns calculated by the modified ABCD matrix with (b) large and (d) small angle incident rays. The gray lines are the trajectories between two neighbor spots (similarly hereinafter).

mirrors were projected onto an  $x$ - $y$  plane. The initial inclination angles and the focal length of the spherical mirror are taken as  $(6.56^\circ, 6.56^\circ)$  and 25 mm, respectively. In all these patterns, the only different parameters for each pattern are the initial entry locations on M1, the mirror spacing, and the pass count under the re-entrant condition, which are given in Table 1. Figure 3(a) gives a morning-glory-like spot pattern in which the “petals” face the “flower heart,” while Fig. 3(d) exhibits a sunflower-like spot pattern in which the “petals” face the outside. More concise spot patterns were obtained by adjusting the mirror spacing and the entry location of the incident ray on M1. Figure 3(b) shows a three-nested-circle spot pattern, while Fig. 3(c) exhibits a seven-nonintersecting-circle spot pattern. For these spot patterns, an angle tolerance of  $\pm 0.3^\circ$

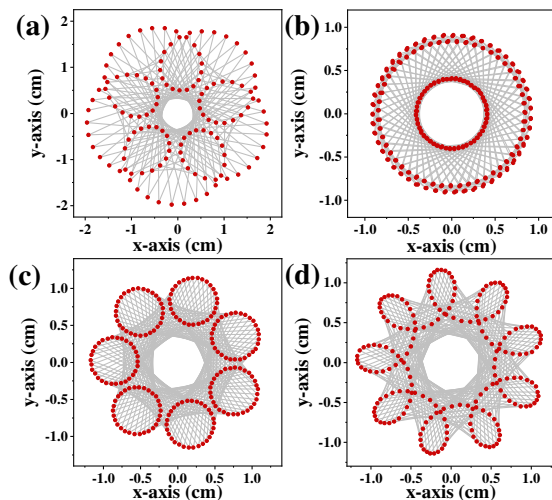


**Fig. 3.** Four exotic spot patterns generated by two-spherical-mirror MPC. (a) A morning-glory-like spot pattern, (b) a three-nested-circle spot pattern, (c) a seven-nonintersecting-circle spot pattern, and (d) a sunflower-like spot pattern. The initial ray parameters for each pattern are listed in Table 1.

is allowed with 2 mm entry and exit holes of light. In order to validate the calculation model, the spot patterns in Figs. 3(a) and 3(c) were simulated by use of TracePro. The results were shown in Fig. 4. The consistency between the calculated and simulated results verifies the validity of the modified ABCD matrix.

With a dense spot pattern, the two-spherical-mirror MPC achieves a long total optical path length, but in a small size. A long total optical path length can improve the detection sensitivity, while a small size not only can enhance the rate of gas exchange and, hence, reduce the response time, but also can realize a compact MPC. The total optical path length  $L$  and the volume  $V$  of each MPC are listed in Table 1. Here the distance from the farthest spot to the original point for each pattern are selected as their mirror radii. The volume is defined as the product of the mirror area and the mirror spacing. The longest optical path length is the seven-nonintersecting-circle spot pattern with a value of 12.92 m in Fig. 3(c), while the smallest volume is the three-nested-circle spot pattern. In fact, a ratio of the total optical path length to the volume can better reflect the space utilization of the ray pattern in a MPC. According to column 7 in Table 1, the most efficient space utilization is the three-nested-circle spot pattern in Fig. 3(b), and the second one is the seven-nonintersecting-circle spot pattern in Fig. 3(c).

The deficiency of the paraxial approximation for these unusual spot patterns results mainly from the large initial inclination angle of the entry ray, which plays an important role in the spot pattern evolution caused by a spherical aberration. When the important ray parameter, the initial inclination angle, remains unchanged, each spot pattern in Fig. 3 can be manipulated to increase the spot density or scale up or down. To increase the spot density, the initial location on M1 ( $x_0, y_0$ ) of the entry ray and the inclination angle ( $x'_0, y'_0$ ) remain unchanged. The focal length  $f$  and mirror spacing  $D$  multiply the intended gain factor. The pass count  $n$  will increase or decrease by the gain factor. For example, the pass count  $n$  in Fig. 3(d) can be two times more (412 times) for the parameters  $f = 50$  mm and  $D = 122.79$  mm, as shown in Fig. 5(a). It should be noted that the increase of the spot density does not occur on the original sunflower-like spot pattern. The new sunflower-like spot pattern in Fig. 5(a) becomes wide and grows two times larger, although the entry location and angle remained unchanged. Moreover, the new and original  $D$ s do not have the exact double relationship, but 1.99 times. In other words, after  $f$  and  $D$  multiply the gain factor, the  $D$  requires fine tuning in order to obtain a new sunflower-like spot pattern since, otherwise, the spot pattern is distorted. A tentative explanation is that there occurs nonlinear calculation processing in Eq. (3).

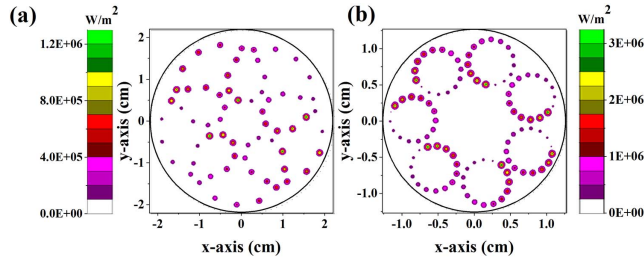
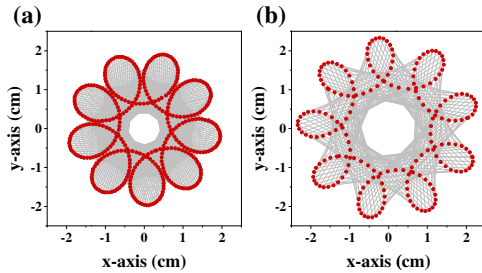
When the inclination angle ( $x'_0, y'_0$ ) of the entry ray remains unchanged, and after the initial entry location ( $x_0, y_0$ ), the focal length  $f$  and mirror spacing  $D$  multiply the same scaling factor simultaneously, the spot patterns can be scaled up or down, as can be seen in Eq. (3). For example, if ( $x_0, y_0$ ),  $f$ , and  $D$  in Fig. 3(d) are increased by a factor of 2, i.e.,  $(6.28, -11.26$  mm),  $f = 50$  mm and  $D = 123.52$  mm, a two times larger similar pattern without any distortions can be obtained with the same pass count  $n$ , as shown in Fig. 5(b).

Due to the nonlinear calculation in Eq. (3), numerical simulations were performed in order to verify if the two-spherical-mirror MPC can meet the re-entrant condition. In other words, the incident ray is able to continue to retrace the same spot

**Table 1.** Initial Entry Location ( $x_0, y_0$ ) on M1, Mirror Spacing (D), and Pass Count Under Re-Entrant Condition ( $\nu$ ) Used to Obtain the Spot Patterns Depicted in Figs. 3(a)–3(d)<sup>a</sup>

Pattern	$(x_0, y_0)$ (mm)	D (mm)	$\nu$	L (m)	V (mL)	RLV (cm <sup>-2</sup> )	$(x_\nu, y_\nu)$ (mm)	$(x'_\nu, y'_\nu)$ (°)
Fig. 3(a)	(8.56, -5.35)	61.16	130	7.95	75.65	10.51	(8.52, -5.51)	(6.55, 6.45)
Fig. 3(b)	(5.60, -6.18)	24.57	306	7.52	6.44	116.77	(5.69, -6.40)	(6.40, 6.37)
Fig. 3(c)	(3.17, -5.54)	61.54	210	12.92	26.42	48.90	(3.19, -5.58)	(6.51, 6.50)
Fig. 3(d)	(3.14, -5.63)	61.76	206	12.72	26.53	47.95	(3.10, -5.55)	(6.63, 6.63)

<sup>a</sup>Total optical pathlength (L), volume of MPC (V), and ratio of L to V (RLV); spot location ( $x_\nu, y_\nu$ ) on M1 and ray inclination angle ( $x'_\nu, y'_\nu$ ) after  $\nu$ th pass count.

**Fig. 4.** Simulations of (a) a morning-glory-like spot pattern and (b) a seven-nonintersecting-circle spot pattern on M2 by use of TracePro. The spot size stands for irradiance.**Fig. 5.** Manipulation of (a) the spot density and (b) the pattern size for a sunflower-like spot pattern with a fixed ray inclination angle.

pattern again and again after every  $\nu$  times pass counts. In this simulation, with a fixed inclination angle ( $6.56^\circ, 6.56^\circ$ ), the mirror spacing D and initial location ( $x_0, y_0$ ) to produce this pattern were adjusted manually in order to make the final ( $x_\nu, y_\nu$ ) and ( $x'_\nu, y'_\nu$ ), as well as the initial ( $x_0, y_0$ ) and ( $x'_0, y'_0$ ) overlap. In fact, the spot patterns in Fig. 3 are those that have been adjusted manually. The last two columns in Table 1 list the spot locations on M1 and ray inclination angles after the  $\nu$ th pass count for the four patterns in Fig. 3. Based on these values, the re-entrant conditions can be met for all four patterns. To understand the re-entrant behavior, a periodic function  $\sin \varphi$  should be paid attention to in the expression of  $x_n$  and  $y_n$ . If  $x'_n$  and  $y'_n$  are linear, a re-entrant trajectory can be achieved for any initial beam parameters. However, a nonlinear function  $\arcsin \varphi$  occurs in  $x'_n$  and  $y'_n$ . The mutual interaction and restriction between  $\arcsin \varphi$  and  $\sin \varphi$  generate periodic patterns and meet the re-entrant condition with some specific initial beam parameters.

In conclusion, we developed a new ABCD matrix without the paraxial approximation, which allows the investigation of a two-spherical-mirror MPC in the presence of a spherical

aberration. The results show that the spherical aberration was accumulated and amplified for each transmission and reflection, producing an abundant set of intricate spot patterns, which are very different from the standard Herriot circle spot pattern. The excellent ratio of the total optical path length to the volume can realize a highly sensitive and compact gas sensor, with a low cost due to the use of a pair of common spherical mirrors. Compact or portable MPCs such as the one described in this Letter have many uses in defense, atmospheric monitoring, and medical diagnostics. Further topics of interest include the fabrication and testing of the two-spherical-mirror MPC, as well as the investigation of the effect of beam interference in the MPC of this type.

**Funding.** National Key R&D Program of China (2017YFA0304203); National Natural Science Foundation of China (NSFC) (61622503, 11434007, 61575113, 61805132); Changjiang Scholars and Innovative Research Team in University of Ministry of Education of China (IRT\_17R70); 111 Project (D18001); Outstanding Innovative Teams of Higher Learning Institutions of Shanxi; Sanjin Scholar (2017QNSJXZ-04); Shanxi “1331KSC”; Robert Welch Foundation (C0568); Foundation for Selected Young Scientists Studying Abroad.

**Acknowledgment.** Frank K. Tittel acknowledges support from the Robert Welch Foundation.

## REFERENCES

1. L. Dong, C. Li, N. P. Sanchez, A. K. Gluszek, R. J. Griffin, and F. K. Tittel, *Appl. Phys. Lett.* **108**, 011106 (2016).
2. Y. C. Cao, N. P. Sanchez, W. Z. Jiang, R. J. Griffin, F. Xie, L. C. Hughes, C. Zah, and F. K. Tittel, *Opt. Express* **23**, 2121 (2015).
3. C. Li, L. Dong, C. Zheng, and F. K. Tittel, *Sens. Actuators, B* **232**, 188 (2016).
4. W. Ren, L. Q. Luo, and F. K. Tittel, *Sens. Actuators, B* **221**, 1062 (2015).
5. K. Liu, L. Wang, T. Tan, G. S. Wang, W. J. Zhang, W. D. Chen, and X. M. Gao, *Sens. Actuators, B* **220**, 1000 (2015).
6. L. Dong, F. K. Tittel, C. Li, N. P. Sanchez, H. Wu, C. Zheng, Y. Yu, A. Sampaolo, and R. J. Griffin, *Opt. Express* **24**, A528 (2016).
7. L. Dong, Y. Yu, C. Li, S. So, and F. K. Tittel, *Opt. Express* **23**, 19821 (2015).
8. J. U. White, *J. Opt. Soc. Am.* **32**, 285 (1942).
9. D. R. Herriott, H. Kogelnik, and R. Kompfner, *Appl. Opt.* **3**, 523 (1964).
10. R. Cui, L. Dong, H. Wu, S. Li, L. Zhang, W. Ma, W. Yin, L. Xiao, S. Jia, and F. K. Tittel, *Opt. Express* **26**, 24318 (2018).
11. J. M. Dang, H. Y. Yu, Y. J. Sun, and Y. D. Wang, *Infrared Phys. Technol.* **82**, 183 (2017).
12. D. R. Herriott and H. J. Schulte, *Appl. Opt.* **4**, 883 (1965).
13. J. A. Silver, *Appl. Opt.* **44**, 6545 (2005).
14. L. Hao, S. Qiang, G. Wu, L. Qi, D. Feng, Q. Zhu, and Z. Hong, *Rev. Sci. Instrum.* **73**, 2079 (2002).
15. S. Ozharar and A. Sennaroglu, *Opt. Lett.* **42**, 1935 (2017).